SUPPLEMENTARY INFORMATION

The Ideal Duo for Salt Formation: Vinpocetine and Tosylic Acid

Ilenia D'Abbrunzo, Francesca Beltrame, Lara Gigli, Nicola Demitri, Cinzia Cepek, Giuseppe Procida, Dario Voinovich, Beatrice Perissutti

Contents

Description	Page N°
Table S1. Fit XPS (N 1s).	**3**
Table S2. Fit XPS (C 1s).	**4**
Table S3. Fit XPS (O 1s).	**5**
Figure S1. Visual appearance of VINPO-PTOS salt powders ground (2h) in the presence of EA (A), ACT (B), ACN (C), MeOH (D), EtOH (E), and H_2O (F).	**6**
Figure S2. PXRD pattern of the VINPO-PTOS salt obtained using LAG (2h) employing different solvents (from top to bottom: HXN, 4-MTHP, EA, ACT, EtOH, MeOH, ACN and H_2O), compared with VINPO and PTOSMH.	**6**
Table S4. Crystallographic data and refinement details for VINPO-PTOS salt at 298 K and 100 K.	**7**
Figure S3. Comparison of the C 1s XPS spectra for pure VINPO (c), the VINPO-PTOS amorphous system (b), and the crystalline (a) VINPO-PTOS salt.	**8**
Figure S4. Comparison of the O 1s XPS spectra for pure VINPO (c), the VINPO-PTOS amorphous system (b), and the crystalline (a) VINPO-PTOS salt.	**8**
Figure S5. HPLC chromatogram of pure VINPO (yellow), crystalline VINPO-PTOS salt obtained by WAG process (blue) and amorphous VINPO-PTOS salt obtained by NG process (green).	**9**
Figure S6. TGA (black) and DSC (red) curves of crystalline VINPO-PTOS salt.	**9**

Figure S7. TGA (black) and DSC (red) curves of amorphous VINPO-PTOS salt.	**10**
Figure S8. Glass transition temperature (T_g) for the amorphous VINPO-PTOS salt detected in the second heating run (heating/cooling/heating cycle).	**10**
Figure S9. Glass transition temperature (T_g) for PTOS MH, detected in the second heating run (heating/cooling/heating cycle).	**11**
Figure S10. FT-IR ATR spectra of VINPO-PTOS crystalline (green) and amorphous (pink) salts, compared to VINPO (blue) and PTOS MH (red). Differences between the two salts spectra are highlighted through light grey rectangles; differences with the starting materials are highlighted through light orange rectangles.	**12**
Figure S11. PXRD of the white solid collected after solubility studies of (initially) amorphous VINPO-PTOS salt	**12**
Figure S12. Physical stability of VINPO-PTOS crystalline salt over time.	**13**
Figure S13. Physical stability of VINPO-PTOS amorphous salt over time.	**13**
Figure S14. Appearance of VINPO-PTOS amorphous salt (yellow) and crystalline salt (white) after 2 hours of storage at 75% RH and 20 °C.	**14**
Figure S15. PXRD of VINPO-PTOS amorphous salt after 2h of exposure to 75% RH.	**14**

Table S1. Fit XPS (N 1s).

VINPOCETINE		
Plot	N1	N11
xc	**400.27946 ± 0.01191**	**398.8759 ± 0.01158**
A	269.13418 ± 3.61111	279.49335 ± 3.6424
Gaussian width	**1.30919 ± 0.02013**	**1.30919 ± 0.02013**
Lorentzian width	**0.4**	**0.4**
Reduced Chi-Sqr	22.79216	
R-Square (COD)	0.99434	
Adj. R-Square	0.99415	

AMORPHOUS SALT		
Plot	N11	N1
xc	**401.70115 ± 0.05238**	**400.55795 ± 0.0503**
A	128.35432 ± 9.87456	177.63961 ± 10.74091
Gaussian width	**1.70532 ± 0.0783**	**1.70532 ± 0.0783**
Lorentzian width	**0.4**	**0.4**
Reduced Chi-Sqr	14.92283	
R-Square (COD)	0.98808	
Adj. R-Square	0.98767	

CRYSTALLINE SALT		
Plot	N11	N1
xc	**402.03821 ± 0.05303**	**400.85734 ± 0.04688**
A	107.23586 ± 7.38943	141.4912 ± 8.09619
Gaussian width	**1.54173 ± 0.08095**	**1.54173 ± 0.08095**
Lorentzian width	**0.4**	**0.4**
Reduced Chi-Sqr	20.45256	
R-Square (COD)	0.97658	
Adj. R-Square	0.97579	

Table S2. Fit XPS (C 1s).

VINPOCETINE			
Plot	**C-C, C-H**	**C-O**	**C=O**
xc	**284.5655 ± 0.03547**	**285.90562 ± 0.17988**	**288.78154 ± 0.12386**
A	4590.97256 ± 208.33977	714.36348 ± 190.95346	378.42857 ± 38.29967
Gaussian width	**1.67204 ± 0.05465**	**1.67204 ± 0.05465**	**1.67204 ± 0.05465**
Lorentzian width	**0.4**	**0.4**	**0.4**
Reduced Chi-Sqr	4555.53302		
R-Square (COD)	0.98502		
Adj. R-Square	0.98457		

AMORPHOUS SALT			
Plot	**C-C, C-H**	**C-O**	**C=O**
xc	**284.55123 ± 0.02536**	**285.92161 ± 0.09286**	**288.75883 ± 0.13883**
A	3139.16926 ± 100.79657	735.0305 ± 89.13488	225.10624 ± 27.69878
Gaussian width	**1.54659 ± 0.04539**	**1.54659 ± 0.04539**	**1.54659 ± 0.04539**
Lorentzian width	**0.4**	**0.4**	**0.4**
Reduced Chi-Sqr	2562.94988		
R-Square (COD)	0.98413		
Adj. R-Square	0.98366		

CRYSTALLINE SALT			
Plot	**C-C, C-H**	**C-O**	**C=O**
xc	**284.53371 ± 0.01583**	**285.93568 ± 0.0629**	**288.35581 ± 0.06482**
A	4623.98259 ± 94.13718	1114.05939 ± 80.56504	594.80046 ± 36.34205
Gaussian width	**1.41476 ± 0.03146**	**1.41476 ± 0.03146**	**1.41476 ± 0.03146**
Lorentzian width	**0.4**	**0.4**	**0.4**
Reduced Chi-Sqr	4592.68019		
R-Square (COD)	0.98761		
Adj. R-Square	0.98724		

Table S3. Fit XPS (O 1s).

VINPOCETINE			
Plot	**OH**	**Carbonates**	**C-O/C=O**
xc	**533.57348 ± 0.02709**	**532.12887 ± 0.02002**	**530.14179 ± 0.13252**
A	1029.63891 ± 29.07399	1725.84747 ± 32.21376	171.41075 ± 19.38785
Gaussian width	**1.52416 ± 0.04032**	**1.52416 ± 0.04032**	**1.52416 ± 0.04032**
Lorentzian width	**0.5**	**0.5**	**0.5**
Reduced Chi-Sqr	594.35296		
R-Square (COD)	0.99226		
Adj. R-Square	0.99198		

AMORPHOUS SALT			
Plot	**C-O/C=O**	**OH**	**Carbonates**
xc	**530.5 ± 0.33176**	**533.68024 ± 0.08042**	**532.15577 ± 0.07303**
A	235.71401 ± 93.88112	938.68325 ± 77.68822	1810.75247 ± 92.6359
Gaussian width	**1.8 ± 0.12711**	**1.8 ± 0.12711**	**1.8 ± 0.12711**
Lorentzian width	**0.5**	**0.5**	**0.5**
Reduced Chi-Sqr	1550.11489		
R-Square (COD)	0.97804		
Adj. R-Square	0.97726		

CRYSTALLINE SALT			
Plot	**C-O/C=O**	**Carbonates**	**OH**
xc	**530.74585 ± 0.19176**	**532.20279 ± 0.05605**	**533.64848 ± 0.05048**
A	480.66249 ± 117.23869	2684.00477 ± 101.61352	1659.72994 ± 90.34634
Gaussian width	**1.53041 ± 0.08549**	**1.53041 ± 0.08549**	**1.53041 ± 0.08549**
Lorentzian width	**0.5**	**0.5**	**0.5**
Reduced Chi-Sqr	3859.76878		
R-Square (COD)	0.97829		
Adj. R-Square	0.97764		

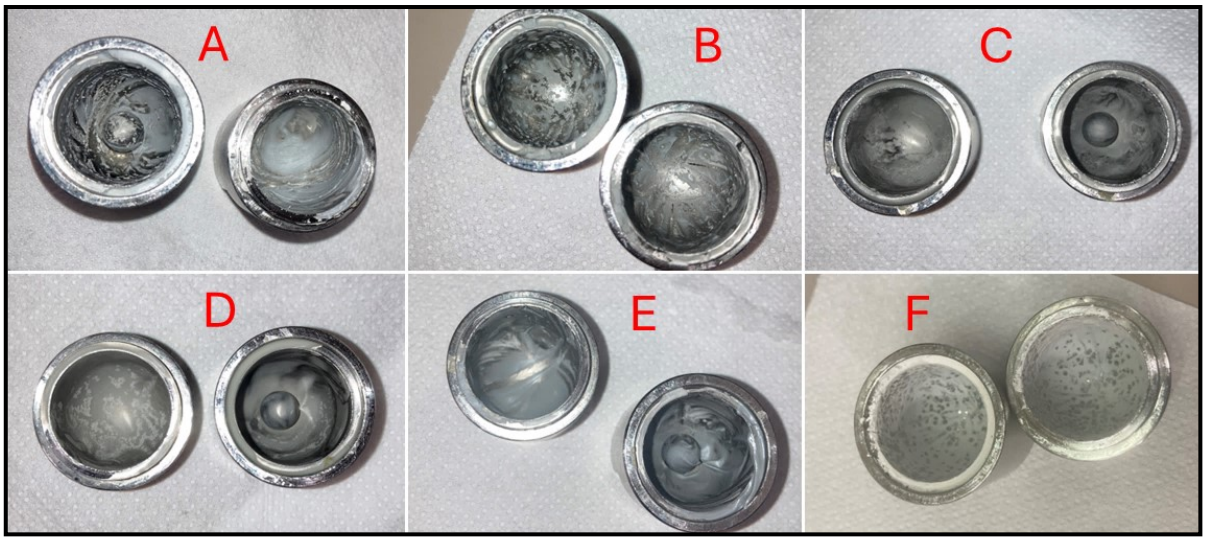

Figure S1. Visual appearance of VINPO-PTOS salt powders ground (2h) in the presence of EA (A), ACT (B), ACN (C), MeOH (D), EtOH (E), and H_2O (F).

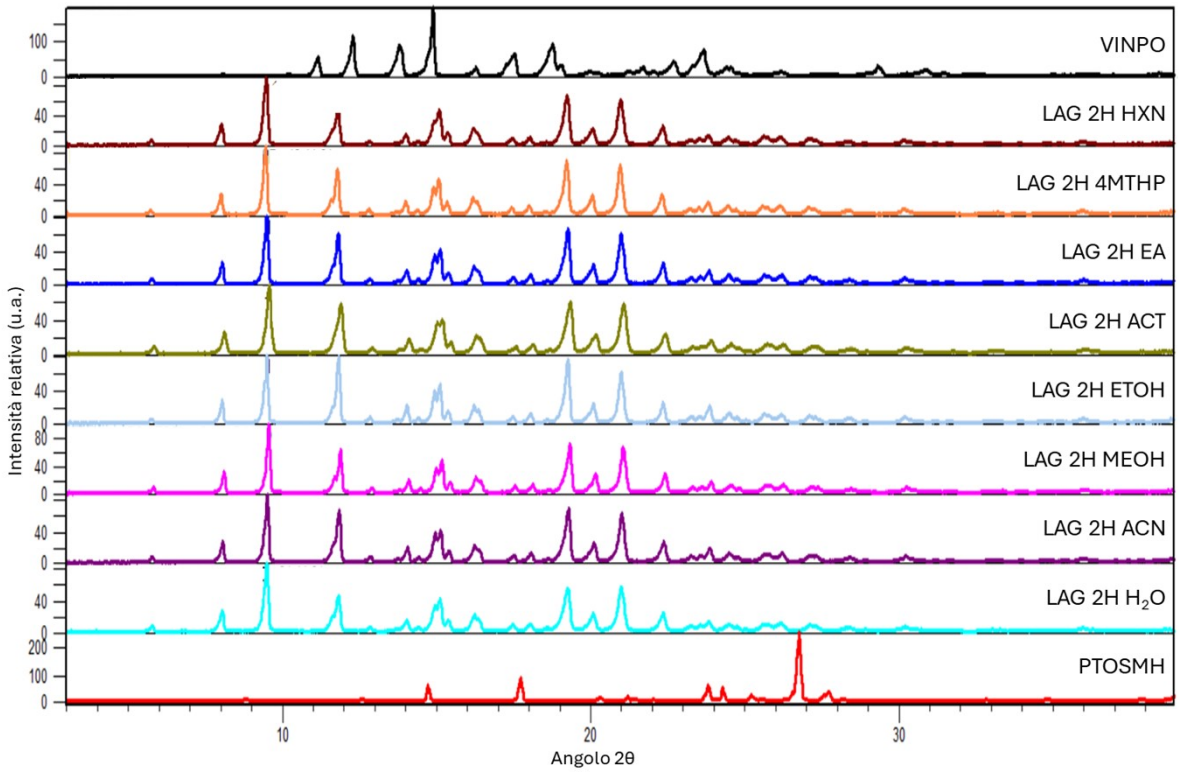

Figure S2. PXRD pattern of the VINPO-PTOS salt obtained using LAG (2h) employing different solvents (from top to bottom: HXN, 4-MTHP, EA, ACT, EtOH, MeOH, ACN and H_2O), compared with VINPO and PTOSMH.

Table S4. Crystallographic data and refinement details for VINPO-PTOS salt at 298 K and 100 K.

	VINPO-PTOS (298 K)	**VINPO-PTOS (100 K)**
Chemical Formula	$[C_{22}H_{27}N_2O_2](C_7H_7SO_3)$	$[C_{22}H_{27}N_2O_2](C_7H_7SO_3)$
Formula weight	522.64 g/mol	522.64 g/mol
Temperature	298(2) K	100(2) K
Wavelength	0.620 Å	0.620 Å
Crystal system	Orthorhombic	Orthorhombic
Space Group	$P\,2_12_12_1$	$P\,2_12_12_1$
Unit cell dimensions	a = 7.644(2) Å	a = 7.657(2) Å
	b = 11.612(2) Å	b = 11.515(2) Å
	c = 30.133(6) Å	c = 29.672(6) Å
	α = 90°	α = 90°
	β = 90°	β = 90°
	γ = 90°	γ = 90°
Volume	2674.7(9) Å^3	2616.2(9) Å^3
Z	4	4
Density (calculated)	1.298 g·cm^{-3}	1.327 g·cm^{-3}
Absorption coefficient	0.115 mm^{-1}	0.118 mm^{-1}
F(000)	1112	1112
Theta range for data collection	1.2° to 31.2°	1.2° to 31.2°
Index ranges	-11 ≤ h ≤ 11,	-12 ≤ h ≤ 12,
	-19 ≤ k ≤ 19,	-19 ≤ k ≤ 19,
	-50 ≤ l ≤ 50	-49 ≤ l ≤ 49
Reflections collected	62797	62713
Independent reflections (data with I>2σ(I))	11945 (11334)	11926 (11584)
Resolution	0.60 Å	0.60 Å
Data multiplicity (max resltn)	8.38 (5.23)	8.86 (5.21)
I/σ(I) (max resltn)	34.14 (13.92)	30.26 (16.99)
Rmerge (max resltn)	0.0464 (0.1175)	0.0526 (0.0818)
Data completeness (max resltn)	92.8% (80.6%)	94.8% (85.6%)
Refinement method	Full-matrix LS on F^2	Full-matrix LS on F^2
Data/restraints/parameters	11945 / 0 / 338	11926 / 0 / 338
Goodness-of-fit on F^2	1.027	1.032
Δ/σ_{max}	0.000	0.002
Final R indices [I>2σ(I)]	R_1 = 0.0550 wR_2 = 0.1524	R_1 = 0.0337 wR_2 = 0.0928

R indices (all data)	$R_1 = 0.0570$ $wR_2 = 0.1566$	$R_1 = 0.0346$ $wR_2 = 0.0939$
Flack x parameter	0.02(1)	-0.02(2)
Largest diff peak and hole	0.736 and -0.505 eÅ^{-3}	0.428 and -0.316 eÅ^{-3}
R.M.S. deviation from mean	0.103 eÅ^{-3}	0.061 eÅ^{-3}

$$R_1 = \Sigma \, ||Fo|-|Fc|| \, / \, \Sigma \, |Fo|, \; wR_2 = \{ \Sigma \, [w(Fo^2 - Fc^2)^2] \, / \, \Sigma \, [w(Fo^2)^2] \}^{½}$$

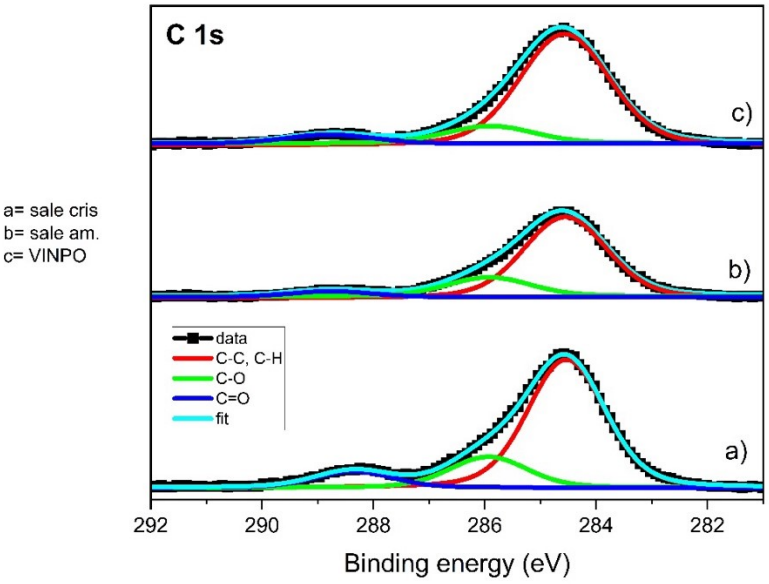

Figure S3. Comparison of the C 1s XPS spectra for pure VINPO (c), the VINPO-PTOS amorphous system (b), and the crystalline (a) VINPO-PTOS salt.

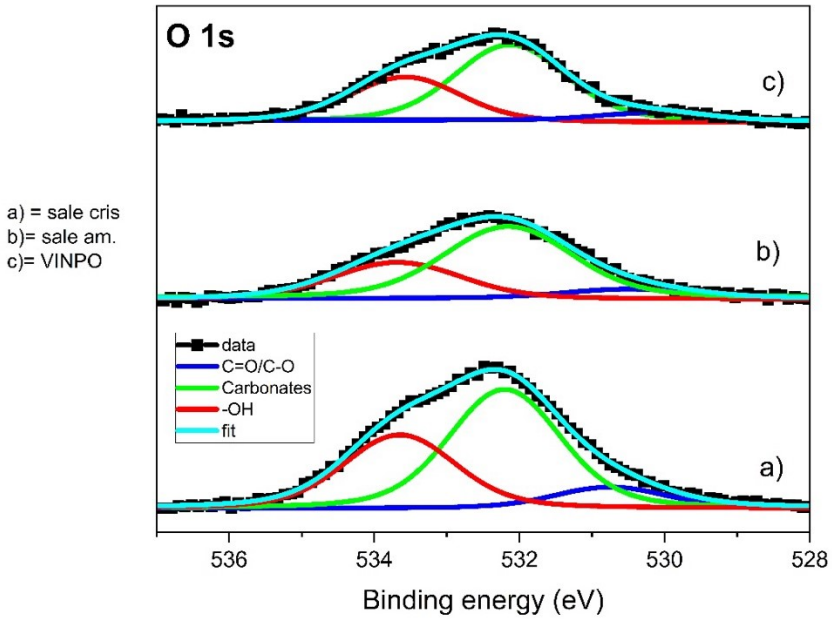

Figure S4. Comparison of the O 1s XPS spectra for pure VINPO (c), the VINPO-PTOS amorphous system (b), and the crystalline (a) VINPO-PTOS salt.

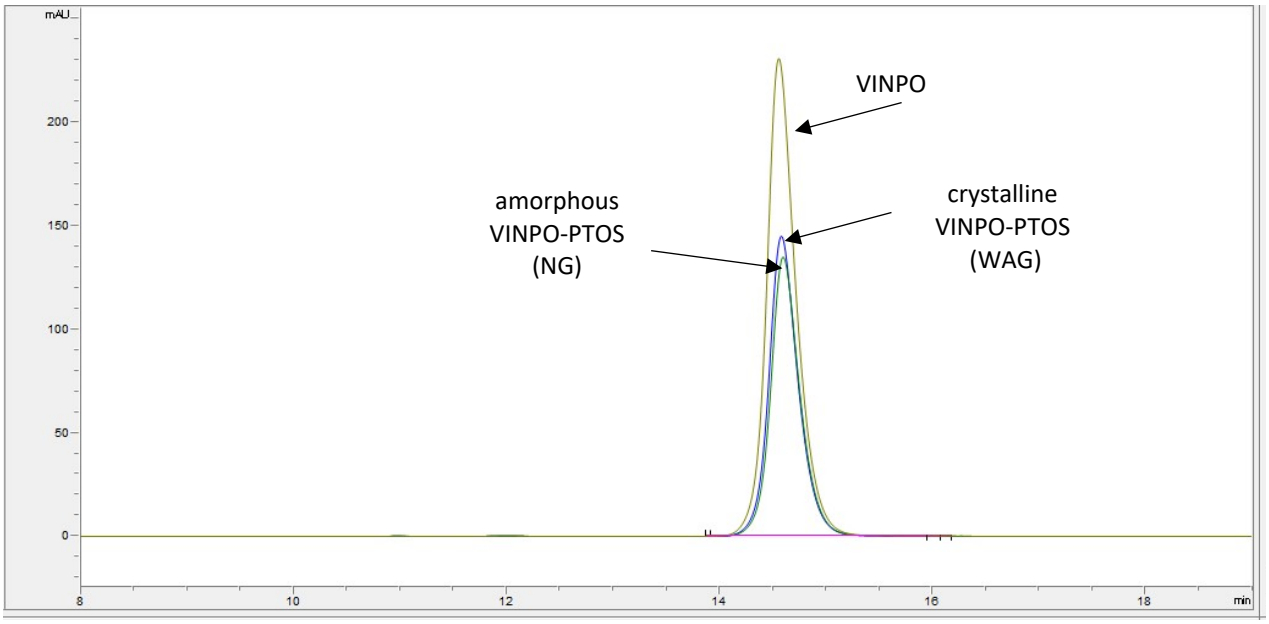

Figure S5. HPLC chromatogram of pure VINPO (yellow), crystalline VINPO-PTOS salt obtained by WAG process (blue) and amorphous VINPO-PTOS salt obtained by NG process (green).

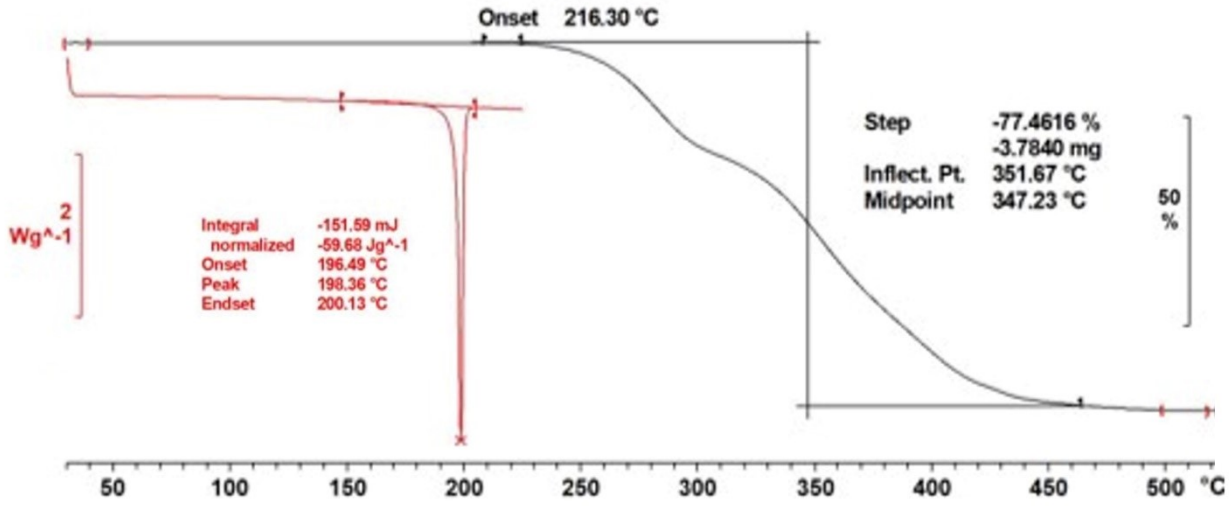

Figure S6. TGA (**black**) and DSC (red) curves of crystalline VINPO-PTOS salt.

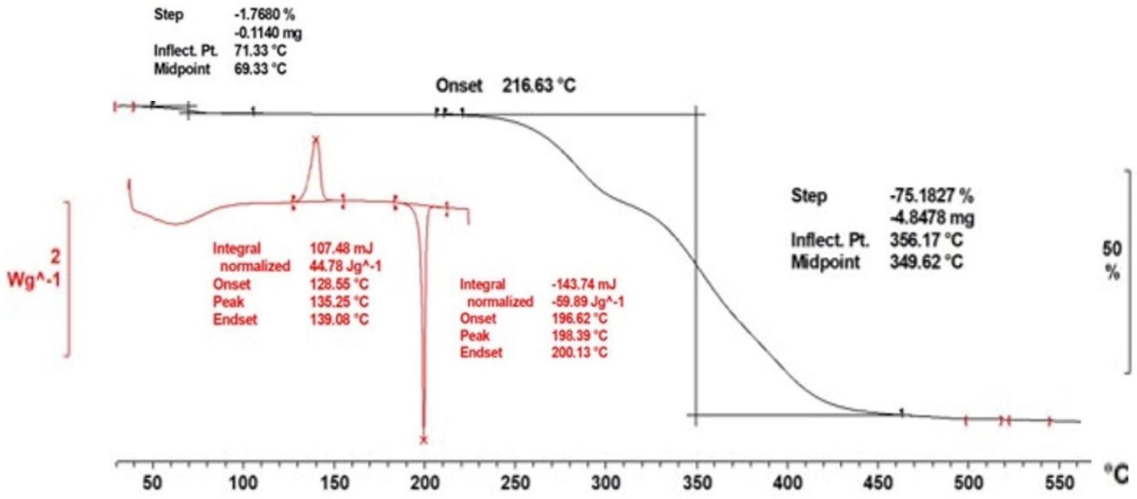

Figure S7. TGA (**black**) and DSC (red) curves of amorphous VINPO-PTOS salt.

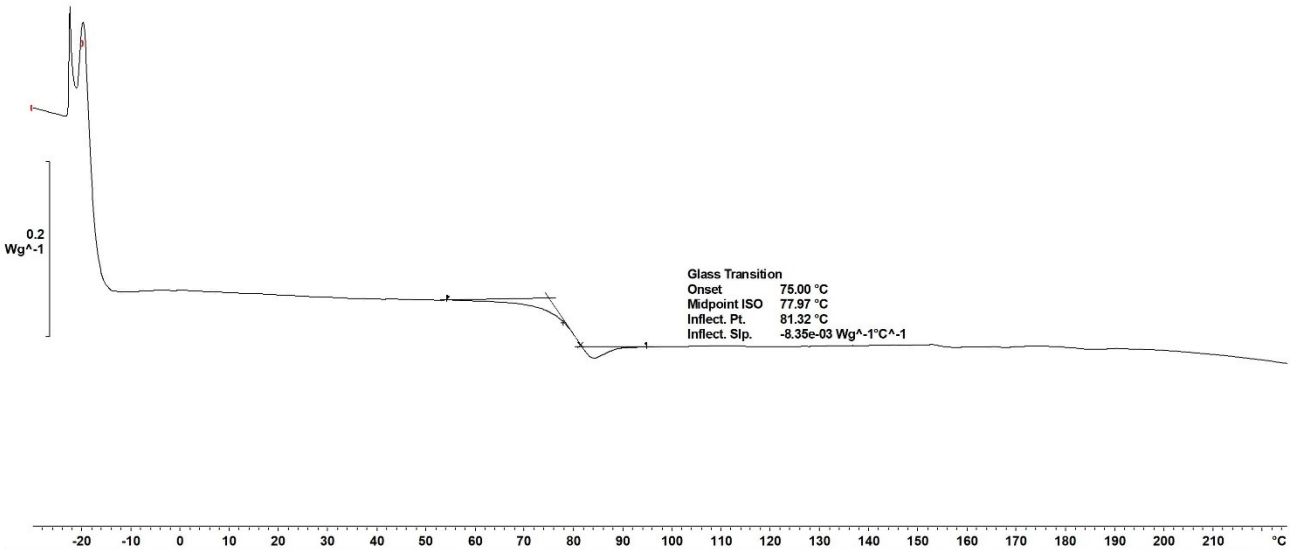

Figure S8. Glass transition temperature (T_g) for the amorphous VINPO-PTOS salt, detected in the second heating run (heating/cooling/heating cycle).

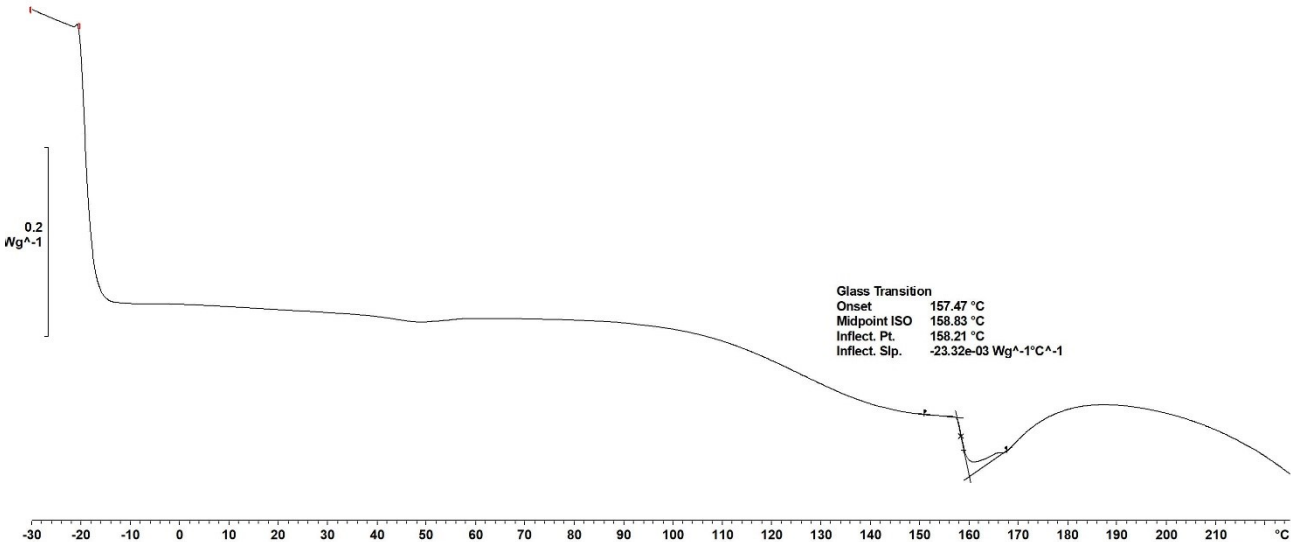

Figure S9. Glass transition temperature (T_g) for PTOS MH, detected in the second heating run (heating/cooling/heating cycle).

FT-IR

The spectra of the two salts are clearly distinguishable from those of the starting materials, which is a typical confirmation of the formation of a new solid phase. It is noteworthy that the spectra of the crystalline and amorphous samples are very similar, suggesting that both solid forms share essentially the same type of intermolecular interactions between the two coformers. Even the characteristic signal broadening typical of amorphous solids is barely visible in the spectrum of this amorphous salt. The most notable differences between the two spectra are as follows: the out-of-plane (C–H) ring bending vibration appears at 835 cm^{-1} in the crystalline salt and shifts to 815 cm^{-1} in the amorphous form (evidenced through the light grey rectangle), similarly to pure PTOS MH. Furthermore, the amorphous salt exhibits characteristic water absorption bands in the 3200 - 3550 cm^{-1} region, mainly due to O-H stretching vibrations. This observation aligns with TGA data, confirming the presence of residual moisture in the solid (light grey rectangle). Compared to the starting materials, the most significant spectral change is the shift of the C=O stretching vibration of VINPO, which moves from 1716 cm^{-1} [1-3] to 1721 cm^{-1} in the crystalline salt and 1723 cm^{-1} in the amorphous form (light orange rectangle). The assignment of the asymmetric (ν_{as}) and symmetric (ν_s) stretching bands of the O-SO3- group proves particularly challenging. Comparison with the spectrum of the starting PTOS MH is not very informative, as the observed signals appear to fall between those reported in the literature for the free acid form of PTOS and its hydrated form, which exhibits three bands at 1310 (ν_{as}), 1292 (ν_{as}) and 1171 (ν_s). Further complicating the interpretation, the 1300 - 980 cm^{-1} region in the salt spectra also contains overlapping signals attributable to VINPO. Given these considerations and based on literature data on the tosylate anion[4], the band at 1136 cm^{-1} in both salts can reasonably be assigned to the asymmetric stretching (ν_{as}) of the O-SO3- group. Similarly, the bands at 1119 cm^{-1} and 1118 cm^{-1} can be assigned to the asymmetric stretching (ν_{as}) in the crystalline and amorphous salts, respectively (light grey rectangle). However, the identification of the symmetric stretching band of the O-SO3- group remain unsolved in both salts. This spectral region is almost identical in the two salts, indicating similar molecular interactions and comparable short-range chemical environments in both solid forms.

1. L. Yu, *Adv Drug Deliv Rev*, 2001, **48**, 27–42.
2. A. Ali, R. Kharshoum and R. Sanad, *Int J Drug Deliv*, 2013, **5**, 167–176.
3. S. A. A. A. Hard, H. N. Shivakumar and M. A. M. Redhwan, *Int J Biol Macromol*, 2023, **253**, 127217.
4. L. Pejov, M. Ristova and B. Šoptrajanov, Spectrochimica Acta Part A: *Molecular and Biomolecular Spectroscopy*, 2011, **79**, 27–34.

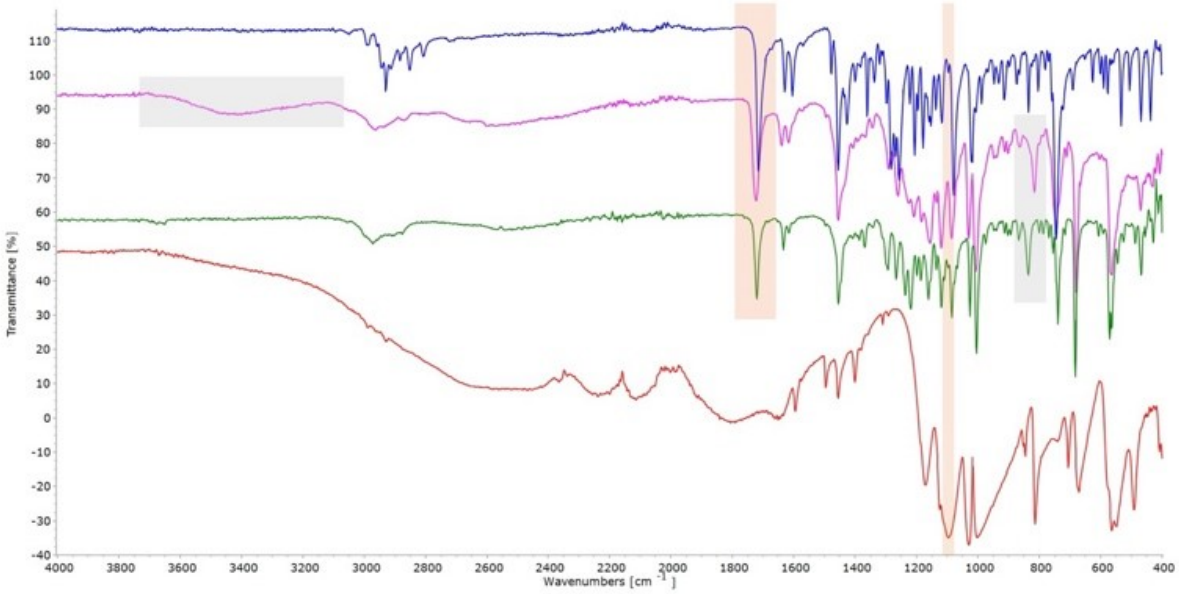

Figure S10. FT-IR ATR spectra of VINPO-PTOS crystalline (green) and amorphous (pink) salts, compared to VINPO (blue) and PTOS MH (red). Differences between the two salts spectra are highlighted through light grey rectangles; differences with the starting materials are highlighted through light orange rectangles.

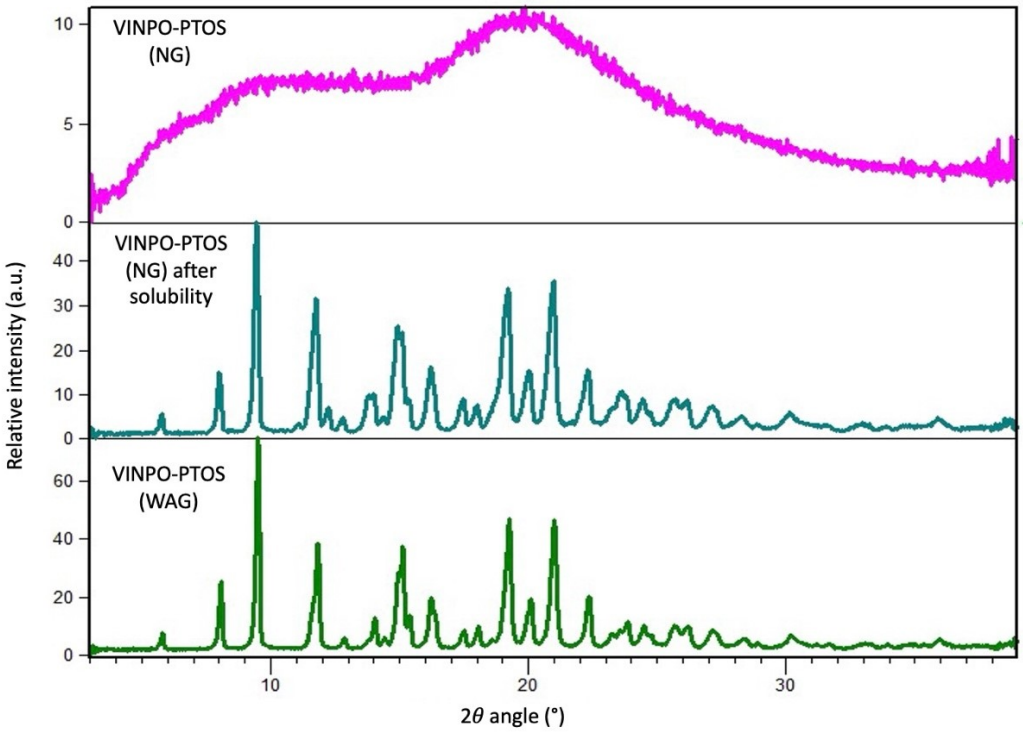

Figure S11. PXRD of the white solid collected after solubility studies of (initially) amorphous VINPO-PTOS salt

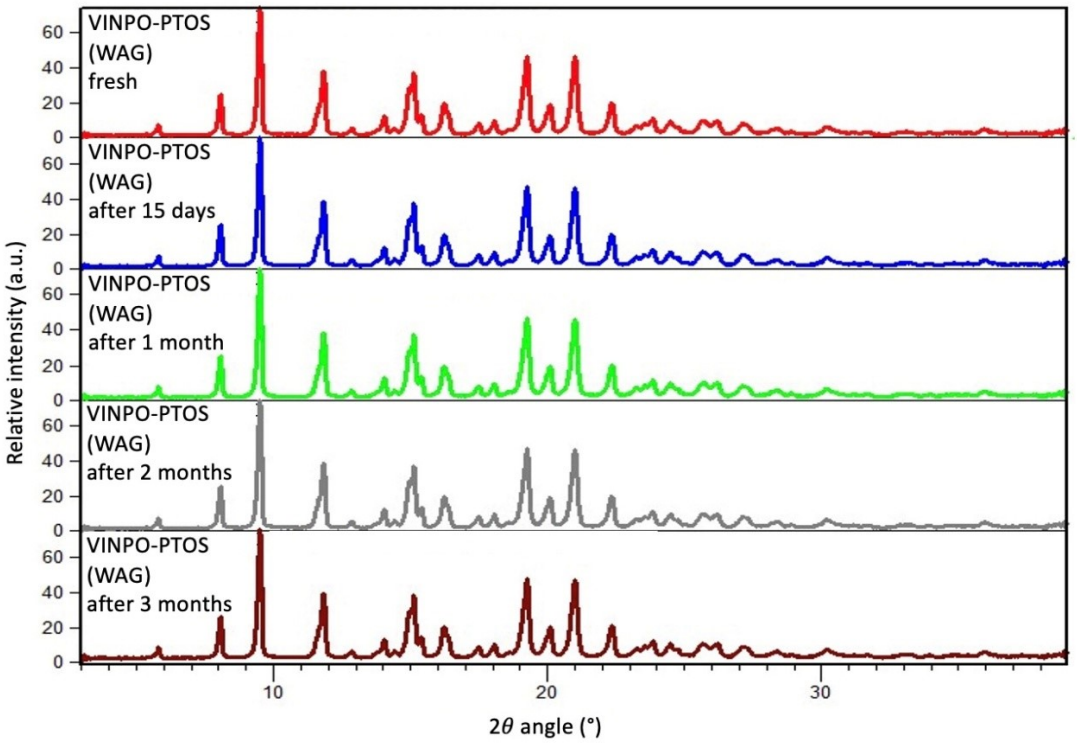

Figure S12. Physical stability of VINPO-PTOS crystalline salt over time.

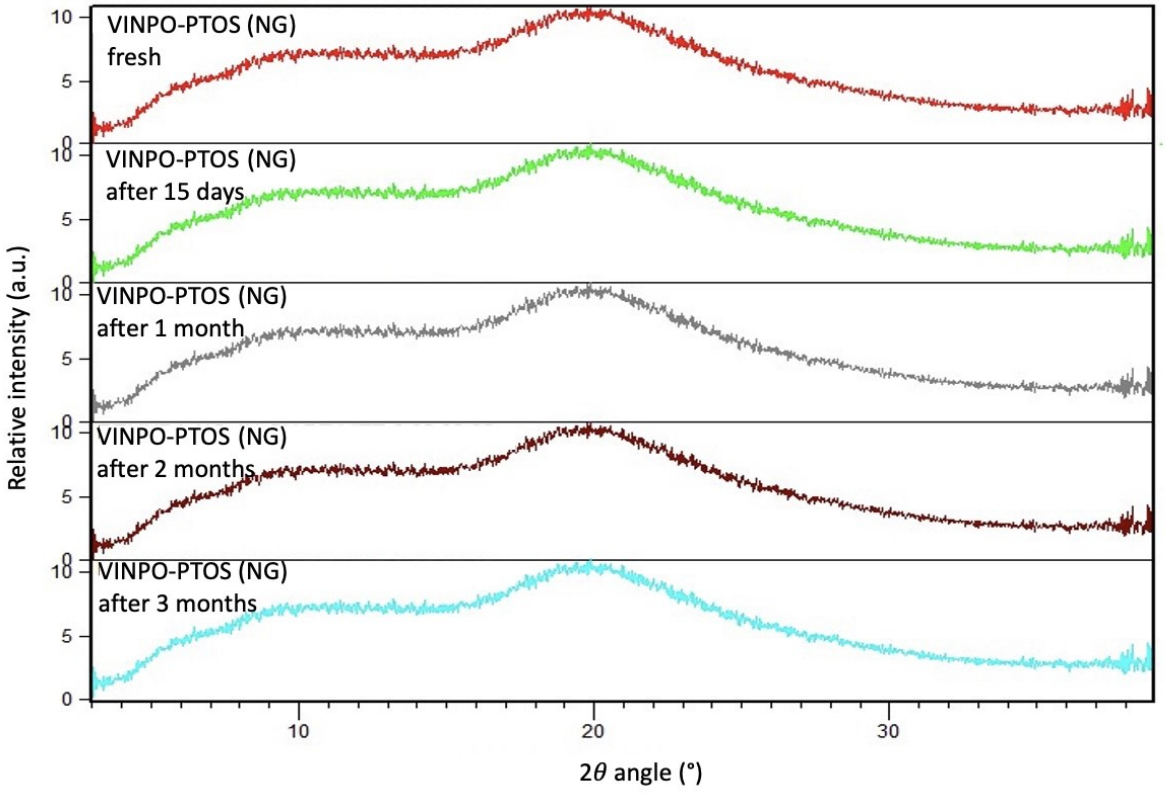

Figure S13. Physical stability of VINPO-PTOS amorphous salt over time.

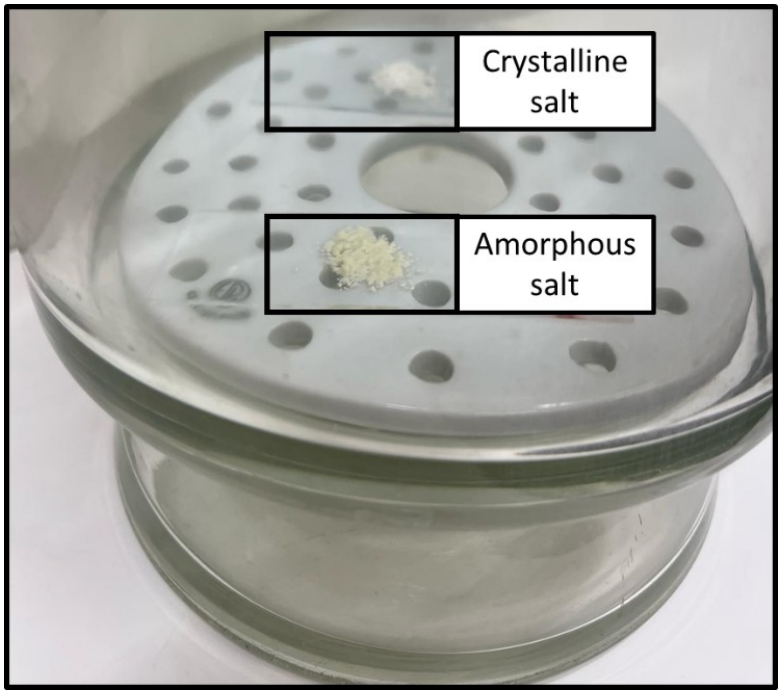

Figure S14. Appearance of VINPO-PTOS amorphous salt (yellow) and crystalline salt (white) after 2 hours of storage at 75% RH and 20 °C.

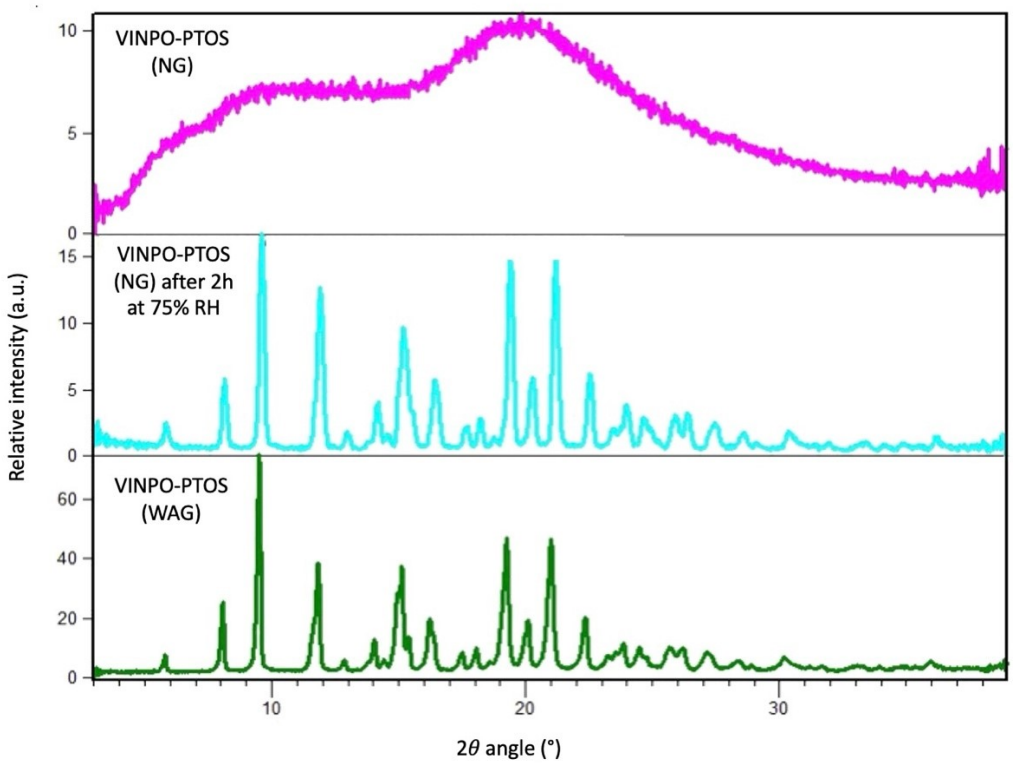

Figure S15. PXRD of VINPO-PTOS amorphous salt after 2h of exposure to 75% RH.